JTTEE5 22:280–289
DOI: 10.1007/s11666-012-9833-3
1059-9630/$19.00 © ASM International

Peer Reviewed

Engineering HVOF-Sprayed Cr_3C_2-NiCr Coatings: The Effect of Particle Morphology and Spraying Parameters on the Microstructure, Properties, and High Temperature Wear Performance

Dominique Poirier, Jean-Gabriel Legoux, and Rogerio S. Lima

(Submitted July 7, 2012; in revised form August 27, 2012)

Chromium carbide-based thermally sprayed coatings are widely used for high temperature wear applications (typical temperature range from 540 to 900 °C). In these extreme environments at those temperatures, several phenomena will degrade, oxidize, and change the microstructure of the coatings, thereby affecting their wear behavior. Although it can be easily conceived that the Cr_3C_2-NiCr coating microstructure evolution after high temperature exposure will depend on the as-sprayed microstructure and spraying parameters, very little has been done in this regard. This study intends to develop a better understanding of the effect of spraying parameters on the resulting chromium carbide coating microstructure after high temperature operation and high temperature sliding wear properties. The microstructures of different coatings produced from two morphologies of Cr_3C_2-NiCr powders and under a window of in-flight particle temperature and velocity values were characterized through x-ray diffraction and scanning electron microscopy. Sliding wear at 800 °C was performed and the wear behavior correlated with the spraying parameters and coating microstructure. Vickers microhardness (300 gf) of the coatings before and after sliding wear was also measured.

Keywords chromium carbide, high temperature wear, HVOF, microstructure, sliding wear testing, spray parameters

1. Introduction

Chromium carbide-based coatings are widely used for high temperature wear applications where tungsten carbides are no longer suitable. Indeed, at temperatures exceeding 540 °C, tungsten carbide coatings' hardness and oxidation resistance drop rapidly (Ref 1). Typical applications for chromium carbide-based coatings include the protection of valves, forming tools, and turbine for power generation (Ref 2). At those temperatures, several phenomena will degrade, oxidize, and change the microstructure of the coatings, thereby affecting their wear behavior. In addition, the high temperatures involved in the spraying processes tend to modify the initial powder phases. During spraying, carbides are partially dissolved, creating a range of Cr composition in the matrix from Cr-rich to the original alloy composition (Ref 3). Furthermore, dissolved carbon may be lost as CO or CO_2 (Ref 4), enhancing formation of degradation phases Cr_7C_3 and $Cr_{23}C_6$. Finally, oxide formation can also occur in flight (Ref 3). Upon quenching of the splats on the substrates, a non-equilibrium microstructure composed of metastable carbides (e.g., Cr_7C_3 and $Cr_{23}C_6$) as well as of partly amorphous and/or nanocrystalline matrix is formed.

Carbide dissolution occurring during spraying has a significant influence on the wear behavior of Cr_3C_2-NiCr coatings. For instance, plasma sprayed coatings typically present extensive carbide dissolution and formation of brittle carbides and oxy-carbides over HVOF or detonation gun spray processes due to the higher particle in-flight temperature and residence time (Ref 5). This together with the higher porosity levels result in coatings with lower hardness displaying poorer performance in impact (Ref 6) and abrasion wear (Ref 7). The nature of the feedstock powder will also affect carbide degradation, and

This article is an invited paper selected from presentations at the 2012 International Thermal Spray Conference and has been expanded from the original presentation. It is simultaneously published in *Thermal Spray 2012: Proceedings of the International Thermal Spray Conference, Air, Land, Water, and the Human Body: Thermal Spray Science and Applications,* Houston, TX, USA, May 21-24, 2012, Basil R. Marple, Arvind Agarwal, Laura Filofteia-Toma, Margaret M. Hyland, Yuk-Chiu Lau, Chang-Jiu Li, Rogerio S. Lima, and André McDonald, Ed., ASM International, Materials Park, OH, 2012.

Dominique Poirier, Jean-Gabriel Legoux, and **RogerioS. Lima**, National Research Council of Canada, 75 de Mortagne Blvd., Boucherville, QC J4B 6Y4, Canada. Contact e-mail: dominique.poirier@cnrc-nrc.gc.ca.

thus wear performance of the coating (Ref 8). In the specific case of erosion wear, a detailed review can be found in Ref 9. Carbide dissolution has a key role in changing the binder hardness as well as the phases present in the coating. It also appears that the resulting supersaturation of the NiCr matrix makes this phase prone to brittle cracking. The erosion behavior is also influenced by other major contributors such as inter-splat adhesion, splat size, level of porosity and cracks, and the presence of oxide stringers.

The as-sprayed metastable coating microstructure can easily evolve when heat is applied, through recrystallization and carbide precipitation for instance (Ref 10). The nucleation and growth of the carbide precipitates will depend not only on the heat treatment temperature and time, but also on the spraying parameters. For instance, an extensive dissolution during spraying will favor precipitation in the form of agglomeration of nucleated carbides, while with minimal dissolution, some growth around the retained carbides will preferentially occur (Ref 10). While those microstructural changes would happen in service for the Cr_3C_2-NiCr coatings intended for high temperature applications, most of the studies replicate this condition by heat treating the coatings prior to testing. It has been shown that carbide precipitation can improve coating wear resistance, adhesion, and hardness (Ref 4, 10, 11). For heat treatment temperatures exceeding 450 °C, significant microstructural changes take place involving loss of the initial carbide structures, carbide precipitation, and gradual formation of a network of carbides where the Ni matrix does not act as a binder anymore. In one study, the coating sliding wear resistance at room temperature was maximized once the heat treatment had resulted in a significant coating hardness increase, but before the formation of the carbide network causing coating brittleness, which corresponded to 1 h at 760 °C for that specific case (Ref 4). In another study, it has been found that heat treatment at 900 °C improves the coating resistance to erosion wear by significantly increasing the ductility of the NiCr matrix phase as well as favoring the inter-splat cohesive strength (Ref 11).

While Cr_3C_2-NiCr coatings are mainly used in high temperature applications, most sliding or abrasive wear tests have been performed at room temperature and typically for one or two sets of spraying parameters only. In this study, two tailored high velocity oxy-fuel (HVOF) Cr_3C_2-NiCr-based powders, exhibiting similar composition but different morphologies, were deposited using the same torch under a window of particle temperature and velocity values. This study intends to develop a better understanding of the effect of spraying parameters on the resulting chromium carbide coating microstructure and high temperature (800 °C) sliding wear properties to ultimately allow proper coating engineering.

2. Experimental Procedure

2.1 Initial Powders

Two commercially available Cr_3C_2-NiCr powders (Sulzer Metco, Westbury, NY, USA) were used in the study. Information on these materials is presented in Table 1. According to the supplier, both powders display a carbide size of about 2-4 μm, i.e., this factor should not influence our results. The volume-weighted powder size distributions were measured using a laser diffraction particle size analyzer (LS320, Beckman Coulter, Miami, FL, USA). The results are shown in Fig. 1.

Micrographs of the two powders are presented in Fig. 2. The 7102 powder is a mixture of spherical and irregular porous particles, whereas the 7305 one is spherical and dense due to the HIP treatment. In all cases, EDS results have shown that white regions in the scanning electron microscopy (SEM) micrograph are composed of Ni and Cr, while darker regions are Cr-carbides.

X-ray diffraction (XRD) analyses of powders and coatings were performed (D8, Bruker AXS, Karlsruhe, Germany). Cr_3C_2 and Ni phases were easily identified in both powders, while peak overlap made detection of Cr_7C_3 and $Cr_{23}C_6$ phases more difficult to confirm.

2.2 Spraying Conditions

An HVOF spray system (DJ2600-hybrid, Sulzer Metco, Westbury, NY, USA) was used with the two powders. Particle velocity and temperature were recorded during spraying (DPV 2000, Tecnar Automation, St. Bruno, QC, Canada), while varying spraying parameters. A total of 27

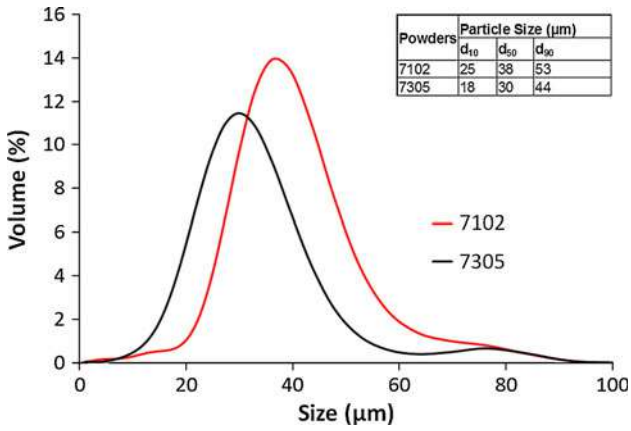

Fig. 1 Powder particle size distribution

Table 1 Details of Cr_3C_2-NiCr powders used in this study

Brand name	Composition, wt.%	Morphology	Nominal particle size
WOKA 7102	Cr_3C_2-20NiCr	Agglomerated and sintered	−45/+15 μm
WOKA 7305	Cr_3C_2-25NiCr	Agglomerated and HIP-treated	−38/+10 μm

spray parameters were tested for each powder within those ranges:

$$100 \leq O_2 \leq 240 \text{ lpm}$$
$$400 \leq H_2 \leq 750 \text{ lpm}$$
$$300 \leq \text{Air} \leq 430 \text{ lpm}$$
$$15 \leq \text{Spraying Distance (SD)} \leq 30 \text{ cm}$$

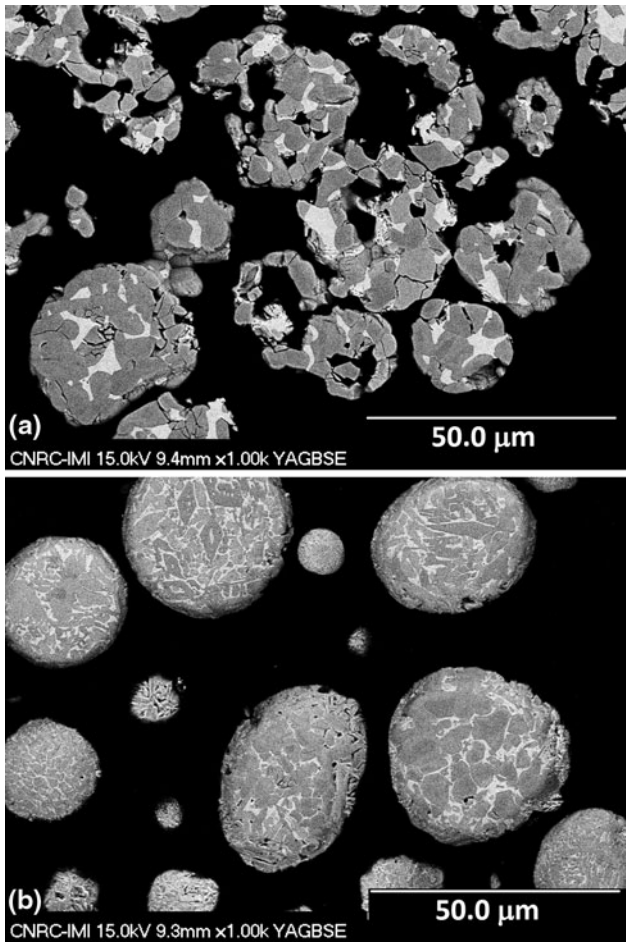

Fig. 2 Cross sections of the feedstock powders: (a) 7102 and (b) 7305

From those, four sets of parameters were selected for each powder so that a wide range of in-flight temperature (T) and velocity (V) values could be used for coating production. In addition, the conditions suggested by the manufacturer of the torch for the production of coatings using cermet powders were also used and are identified by the symbol "&" in Table 2. Figure 3 shows the resulting temperature-velocity graphs for the 7102 and 7305 powders. Each dot represents the particle average temperature and velocity of one set of spraying parameters, and the circled dots represent the five spraying parameters selected for further testing. The set of spraying parameters indicated with an arrow represents the particle average temperature and velocity achieved with the conditions suggested by the DJ2600 manufacturer for the production of cermet coating. For some sets of spray conditions, the velocity and temperature measurements exhibited a bimodal distribution (shown with gray squares on Fig. 3). For those conditions, the temperature-velocity graphs showing the results for each particle clearly presented two distinct peaks. Spraying conditions resulting in such bimodal temperature/velocity distribution were eliminated because this typically leads to heterogeneous coating.

For each set of spraying parameters, four low carbon steel Almen N strip substrates were fixed to a rotating cylinder used as a sample holder. The deposition of four replicate coatings was therefore performed under identical conditions. During spraying, the coating surface temperature was monitored with a pyrometer operating at a wavelength range of 8-14 µm for a calibrated temperature range of 0-500 °C (Mikron M67S, Lumasense, Santa Clara, CA, USA). To minimize residual stresses, a spraying pause was added in between spraying passes (when needed) in order to keep the coating surface temperature below the upper temperature limit fixed at 230 °C. As expected, the spraying parameters leading to higher in-flight particle temperature required longer spraying pauses, whereas the colder conditions did not necessitate any. All coating thicknesses obtained were between 285 and 330 µm. After deposition, the deflection of each Almen strip was measured and normalized for a 300-µm thickness. One Almen strip per condition was cut for metallographic preparation and further characterization, i.e., SEM observation, XRD, and microhardness.

For the five sets of spraying parameters, the deposition efficiency (DE) was calculated from the change in weight

Table 2 Spraying parameters

Powder	Set	O_2, lpm	H_2, lpm	Air, lpm	SD, cm	T, °C	V, m/s	DE, %
7102	1*	236	400	300	15	2057	849	12
	2	230	600	380	25	1805	635	35
	3	200	750	300	25	1816	737	38
	4&	231	684	372	20	1774	810	40
	5	100	400	300	15	1650	674	49
7305	1*	236	400	300	15	1838	761	20
	2	200	600	300	20	1705	679	48
	3&	231	684	372	20	1695	765	50
	4*	200	400	430	15	1707	801	25
	5	100	400	300	15	1587	544	47

* Condition eliminated, DE below 30%
& Manufacturer condition

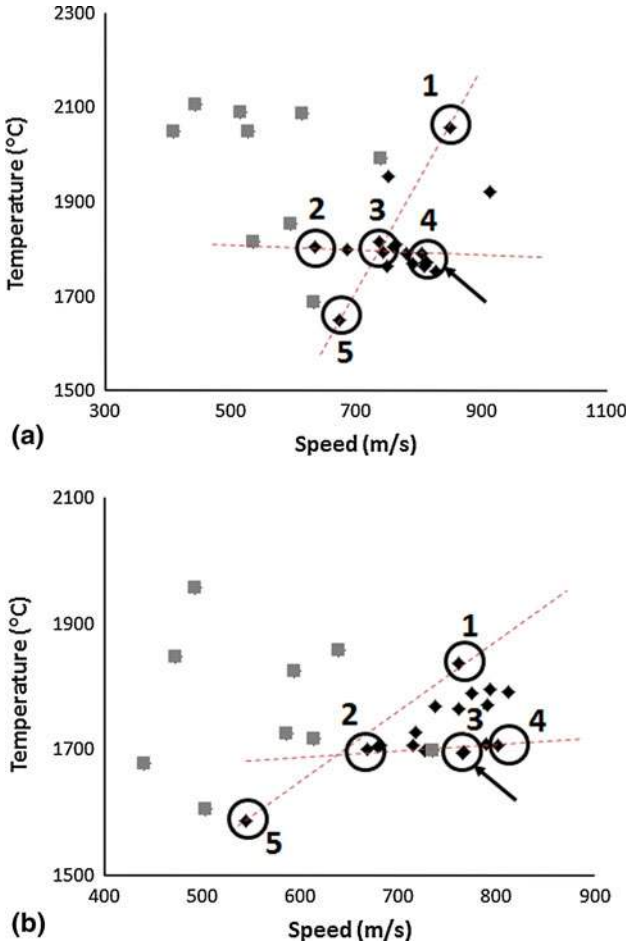

Fig. 3 Mean temperature/velocity plot for different spraying conditions: (a) 7102 and (b) 7305

of the low carbon steel grit-blasted substrates before and after deposition with respect to the powder feedrate. Spraying parameters with DE values below 30% were considered as not viable and eliminated from further testing. The parameters eliminated are identified by an asterisk (*) in Table 2.

2.3 Characterization

Powder and coating microstructures were observed using field emission SEM (S4700, Hitachi Instruments Inc., Tokyo, Japan). Samples were prepared using standard metallographic procedures to produce a polished cross section. Porosity levels were evaluated from image analysis on ten images obtained with the backscattered mode of an SEM equipment (JSM-6100, JEOL, Tokyo, Japan) under conditions of contrast to enhance the pores. The phases present within the various powders and coatings as well as crystallinity indices (I_c) were determined by XRD using a Bruker D8 Discover x-ray diffractometer (Madison, WI, USA) with Cu-Kα1 radiation at 1.6 kW. A step size of 0.05° with a time length of 2.5 s was selected, for a range of 20-70°. I_c is defined in this paper as the ratio of the areas of the Bragg peaks over the total areas of the

Table 3 Wear tests conditions

Parameters	Values
Ball material	Al_2O_3
Load	100 N
Linear sliding speed	0.25 m/s
Sliding distance	1000 m
Test temperature	RT or 800 °C (both under air)

spectrum between 30° and 55° (Ref 12). Vickers microhardness average values (Micromet II, Buehler, Lake Bluff, IL, USA) were obtained from ten indentations performed on the cross section of the coatings. Wear test samples were prepared by spraying the Cr_3C_2-NiCr powders on 5-cm diameter SS310 disks. The coatings produced, of about 500 μm in thickness, were then ground and polished to reach a flat and mirror-like surface finish with a R_a of ~0.4 μm (Surftest-211 stylus profilometer from Mitutoyo, Kawasaky, Japan). Wear tests were performed with a universal macro-tribometer (UMT-2MT, CETR, Campbell, CA, USA) using the ball-on-disk configuration. Most sliding tests were performed at 800 °C, but some coatings were also submitted to room temperature (RT) sliding tests for comparison purposes. The wear test conditions are listed in Table 3. The obtained volume losses were measured with an optical profilometer (uCAM-3D, Novacam Technol. Inc, Pointe Claire, QC, Canada).

3. Results and Discussion

3.1 As-Sprayed Coatings

Several as-sprayed coating properties are summarized in Table 4. As expected, negative Almen deflection values tend to be obtained from spraying conditions with higher in-flight particle velocity (Table 2). The peening effect of the high velocity incoming particle induces compressive residual stresses in the coatings. All coatings display similar hardness values of about 1050 HV, except the 7102-5 coating, for which the higher level of porosity leads to a lower hardness value. For all other spraying parameters, the variation in porosity values is within the error margins and as a consequence, nonsignificant.

Figure 4 exhibits the XRD patterns obtained from the 7102 and 7305 feedstock powders as well as the coatings resulting from the different spraying conditions. The different phases are indicated in the figure. While Bragg peaks are well defined in the case of the feedstock powder, a significant peak broadening is obtained after spraying for all conditions due to the dissolution of the carbides and the presence of amorphous/nanostructured phases in the coatings (Ref 12). While it is difficult to visually evaluate the extent of dissolution by comparing those patterns, the calculation of I_c was found to allow easy comparison between the spraying conditions. The lower the I_c value, the higher the extent of carbide dissolution. The I_c values for all coatings are listed in Table 4 and can be compared with the I_c values of the 7102 and 7305 feedstock powders of 0.93 and 0.81, respectively. A higher in-flight particle

Table 4 As-sprayed coating properties

Powder/set	Almen deflection (a), μm ($n = 4$)	Porosity % ($n = 10$)	HV 300 gf ($n = 10$)	I_c
7102/2	86 ± 27	1.2 ± 0.2	1051 ± 127	0.47
7102/3	−21 ± 33	1.6 ± 0.2	1061 ± 66	0.50
7102/4	−109 ± 44	1.4 ± 0.2	1052 ± 109	0.50
7102/5	85 ± 14	5.5 ± 0.4	940 ± 63	0.65
7305/2	28 ± 28	1.1 ± 0.2	1024 ± 46	0.42
7305/3	−52 ± 29	1.2 ± 0.2	1067 ± 40	0.43
7305/5	105 ± 18	1.5 ± 0.4	1010 ± 73	0.53

(a) Almen deflection normalized for 300-μm thickness. A negative number indicates a compressive residual stress

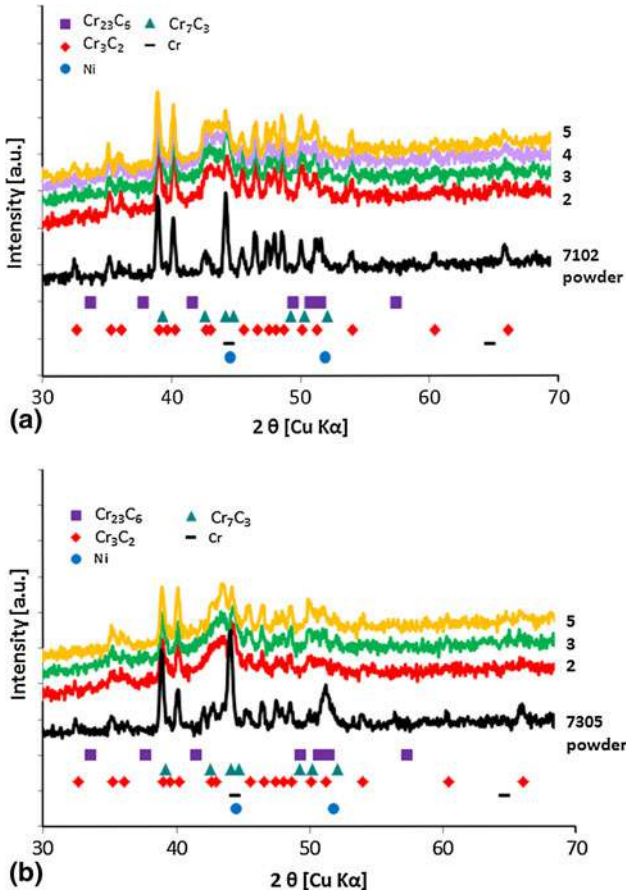

Fig. 4 XRD patterns of (a) 7102 and (b) 7305 feedstock powders and their as-sprayed coatings

temperature results in lower I_c levels due to a greater degradation of the powder. The overall lower I_c values obtained with the 7305 could be due to the lower initial I_c of the powder. However, it should also be considered that the DPV 2000 is measuring the surface temperature of the in-flight particles. As the 7305 ones are denser, it is probable that the conductivity of this powder is higher, leading to higher temperatures inside the particles.

From observation of the microstructures of the different coatings produced with the 7102 powder (Fig. 5), it appears that the spraying process is robust as uniform coatings, made of a homogeneous distribution of Cr_3C_2 (in dark gray) in the NiCr matrix (in light gray), are obtained for all conditions. Set 4 (Fig. 5c), which was the spraying condition leading to the highest particle velocity, has produced a coating exhibiting the highest level of interface adhesion. On the opposite, the largest gaps at the interface were obtained with Set 5 (Fig. 5d), which was the ''coldest'' condition. This coating is also more porous. This is to be expected as a lower in-flight particle temperature decreases the proportion of liquid phase and plastic behavior and thus the particle deformability. On the other hand, a higher concentration of intact carbides is visible. This observation, together with the higher I_c value for this condition, indicates a lower amount of carbide dissolution due to the lowest in-flight particle temperature. Set 5 is also the condition where the highest DE was obtained. It is hypothesized that low particle temperature levels will significantly increase the viscosity of the particle, which would yield lower rates of carbide rebounding upon impact with the substrate. Set 3 and 4 were found to display similar microstructures, hardness, and I_c values. Set 3 was therefore eliminated from further testing.

The microstructures of the coatings produced using the 7305 powder are shown in Fig. 6. It is seen that this powder also leads to dense and uniform coatings with a homogeneous distribution of Cr_3C_2 particles.

Set 5 of the 7305 powder (Fig. 6c), which was the spraying condition leading to the lowest spray distance (i.e., 15 cm) and the ''coldest'' condition, has produced a coating exhibiting the highest level of interface adhesion (i.e., no gaps). Therefore, for this specific powder, the spray distance seems to be a determinant factor for the improvement of coating adhesion.

Similar to the 7102 powder, the ''coldest'' condition, Set 7305-5, leads to a higher concentration of carbides. The high value of I_c obtained indicates a lower extent of carbide dissolution with this condition. However, for this powder, the DE of Set 5 is similar to those obtained with conditions 2 and 3, displaying a lower concentration of carbides (Tables 2, 4). As a consequence, improved carbide retention during spraying would not play a role in the higher carbide content of Set 5 with the 7305 powder. As the 7305 powder is denser than the 7102 powder, it could be that carbide rebounding is reduced, leading to high carbide retention for all conditions with this powder. Compared to the 7102, Set 5 of the 7305 powder produces a coating that is relatively dense, exhibiting no major gaps at the interface with the substrate. The low porosity of this powder could help to produce denser coatings.

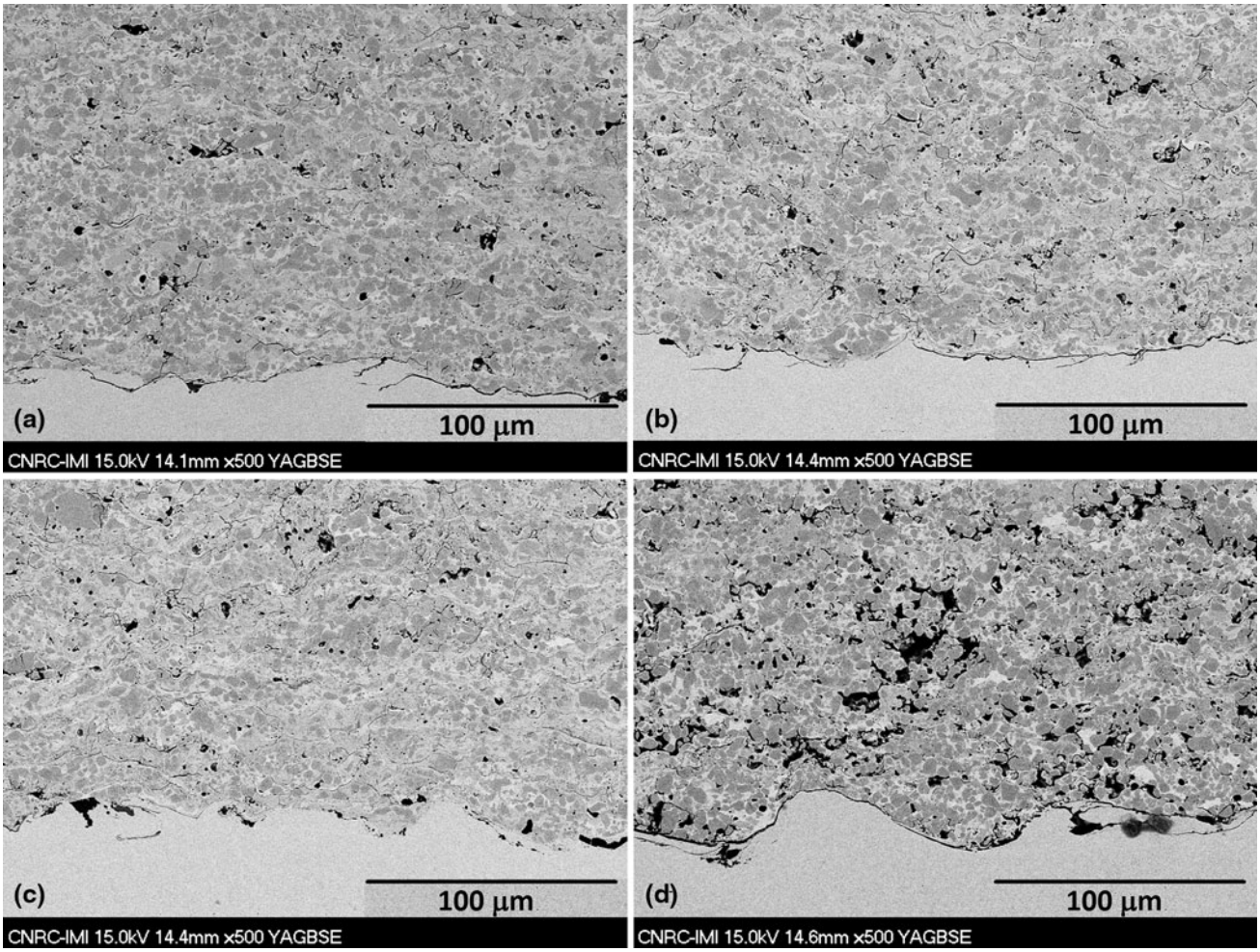

Fig. 5 As-sprayed microstructures of the coatings produced from the spraying of the 7102 powder: (a) Set 2, (b) Set 3, (c) Set 4, and (d) Set 5

3.2 Wear Tests

As expected, the high temperature of the wear tests has allowed an evolution of the as-sprayed, metastable microstructure of the coatings. The XRD peaks of the wear-tested coatings shown in Fig. 7 are well defined and very similar to the feedstock powders, except for the addition of a Cr_2O_3 peak. This peak results from the oxidation of the coating surface during sliding test performed in air. Also, the indices of crystallinity after the test, shown in Table 5, are increased to a level closer to the initial powders. This indicates carbide reprecipitation and crystallisation of amorphous and/or nanocrystalline phases. Figure 8 illustrates the morphology of the carbide precipitates. Compared to the original carbide phase, they are much smaller and appear to be evenly distributed in the matrix.

Carbide precipitation has hardened the worn coatings (Table 4 versus Table 5). They all reach a similar value of about 1300 HV, but for the 7102-Set 5 coating, for which the lower hardness is probably due to its high level of porosity. This high porosity lowers the wear resistance of the coating as well. The effect of those microstructural changes on the coating hardness has been studied in detail in Ref 10. Typically, an initial decrease is observed due to the relief of internal stresses through recovery and recrystallization, a decrease in solid solution strengthening, and an increase in grain size. Once carbides start to precipitate, the trend is reversed and coating hardness rises to values exceeding the coating initial hardness. At this point, a ''sintering'' effect could also contribute to the hardness increase by improving adhesion between splats and by decreasing porosity levels. Then, the hardness values can either plateau due to overaging or keep increasing due to the formation of a carbide network. Oxides have an ambiguous effect: They are themselves harder than the matrix, but they could also reduce splat-splat bonding.

Friction coefficients (COF) obtained by the 800 °C ball-on-disks wear tests are similar for the two powders and all spraying conditions and correspond to what have been observed elsewhere (Ref 13). All coatings also display similar wear mechanisms. Figure 9 shows the wear track of the coating 7102-Set 2. The large number of

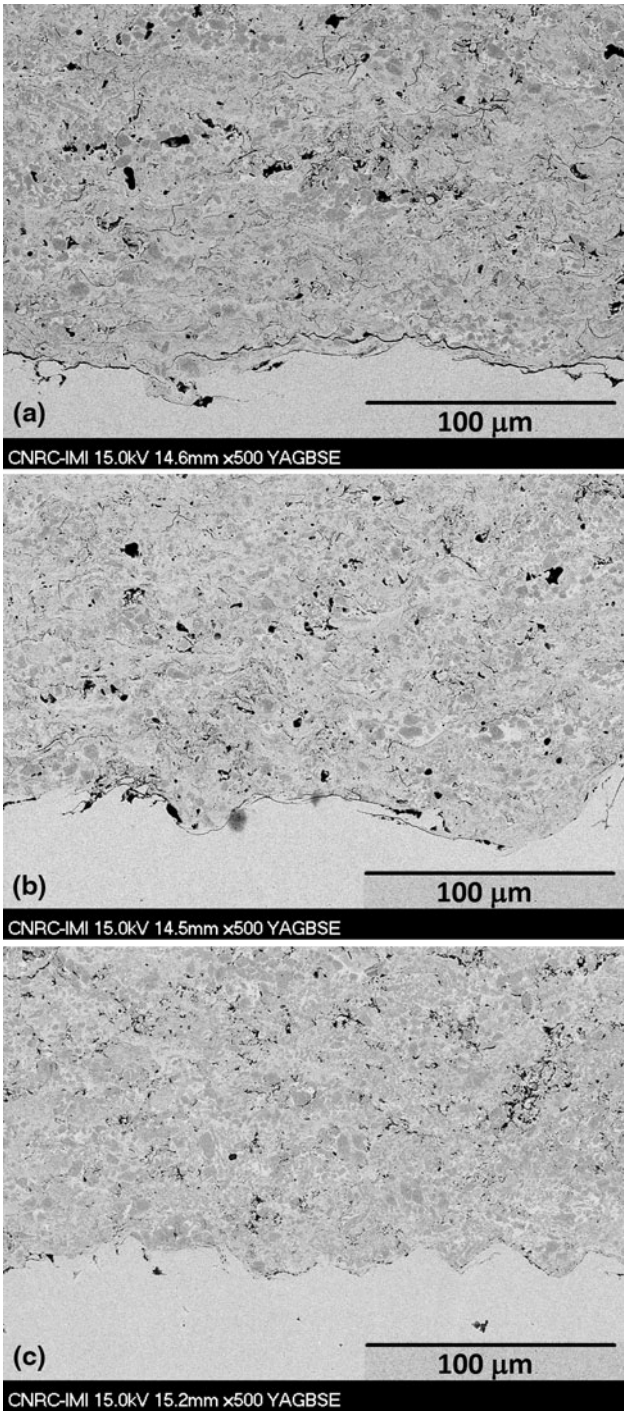

Fig. 6 As-sprayed microstructures of the coatings produced from the spraying of the 7305 powder: (a) Set 2, (b) Set 3, and (c) Set 5

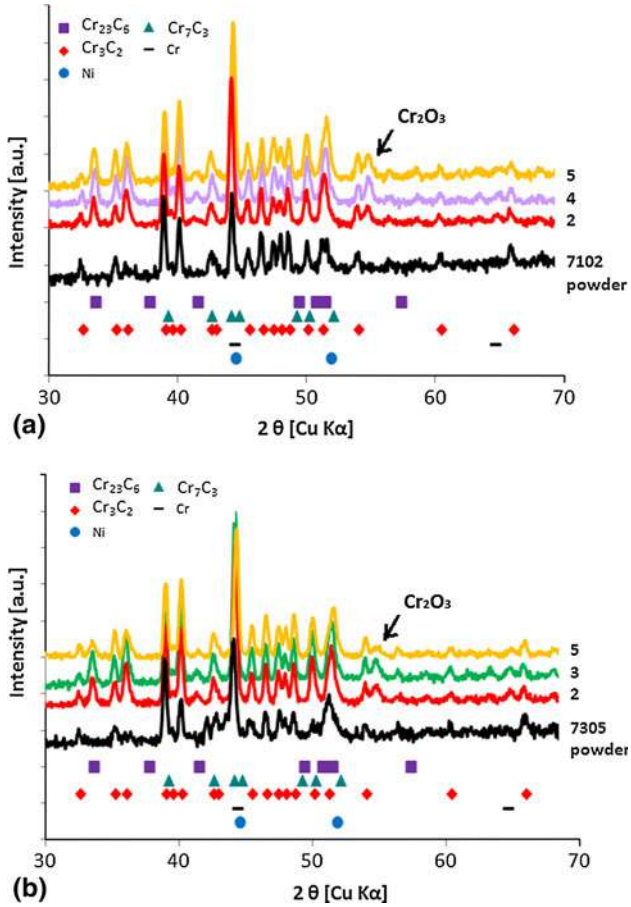

Fig. 7 XRD patterns of (a) 7102 and (b) 7305 feedstock powders and their coatings after sliding wear test at 800 °C

parallel scratches seen in Fig. 9 indicates that the abrasive wear is an important mechanism. In the close-up micrograph, the smooth regions shown by arrows are representative of the large carbides. The size and morphology of those smooth regions are indeed very similar to the large carbides visible in Fig. 8. EDS analysis has shown a systematic increase in oxygen of about 2% in the wear track compared to the unworn coating surface. This could indicate that the harder oxides resist wear more than the other phases so that they preferentially appear at the surface of the wear track. The heat generated during the wear test could also lead to preferential oxidation in those areas.

For powder 7102, the spraying Set 4 exhibits a lower volume loss than Set 2. While the HV, I_c, and wear tracks of those two coatings are comparable, the residual stresses are the opposite. It seems that the Set 4 compressive residual stresses improve the coating wear resistance.

Figure 10 shows the relationship between volume loss and normalized Almen strips for the two powders. It appears that the residual stresses are a key factor for the CrC-NiCr coating high temperature wear behavior. However, it is most probable that the residual stresses are released during the heating stage prior to the wear testing. If this is the case, they cannot be the direct explanation of this variation in wear properties. In order to confirm this aspect, the different coatings produced with the 7102 powder were also submitted to sliding wear at RT (results presented in the two last columns of Table 5). As expected, the volume losses are higher at room temperature than at 800 °C: Without heat treatment, carbide precipitation does not occur and the coating hardness

Table 5 Wear-tested (800 °C) coating properties

Powder/set	COF	Volume loss, mm^3 ($n = 2$)	HV 300 gf (a) ($n = 10$)	I_c (a)	COF RT	Volume loss RT, mm^3 ($n = 2$)
7102/2	0.25 ± 0.02	5.8 ± 0.9	1303 ± 67	0.93	0.49 ± 0.09	7.3 ± 1.5
7102/4	0.27 ± 0.02	3.7 ± 0.4	1308 ± 75	0.92	0.44 ± 0.08	7.2 ± 1.9
7102/5	0.26 ± 0.02	8.3 ± 2	1035 ± 86	0.86	0.47 ± 0.07	18.4 ± 1.3
7305/2	0.24 ± 0.02	7.0 ± 0.4	1266 ± 124	0.94	…	…
7305/3	0.26 ± 0.02	6.4 ± 0.7	1278 ± 72	0.86	…	…
7305/5	0.25 ± 0.02	10.7 ± 0.4	1177 ± 170	1.04	…	…

(a) Measured after sliding wear test at 800 °C

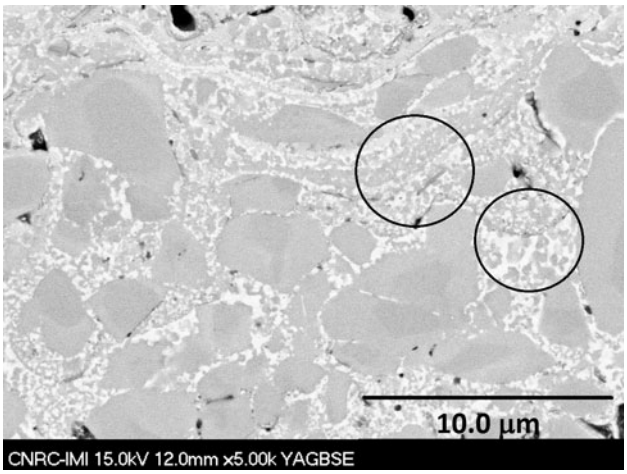

Fig. 8 Microstructure of 7102-Set 2 coating after sliding wear test at 800 °C. Gray precipitated carbides can be seen in the white matrix, as highlighted

stays lower. The COF obtained at RT are also twice those obtained at 800 °C. This difference in behavior has been attributed to the softening of the coating material and the reduction of its work hardening ability at high temperatures (Ref 2). However, contrary to what is seen at high temperature, both the 7102-2 and 7102-4 coatings are showing similar volume losses for RT sliding wear. This confirms the fact that residual stresses are not the direct cause for the improvement of sliding wear performance at high temperature. Even though the residual stresses are not the direct cause of wear property variation, it is still possible that residual stresses drive some sort of change in the heating stage of the sliding test, leading to a strong effect regarding the sliding wear property performance.

Two hypotheses are suggested to explain this phenomenon. It is first hypothesized that the residual stresses affect the sintering behavior of those coatings upon heating. A compressive residual stress generates an internal pressure that would promote the diffusion process at the origin of splat cohesion and porosity reduction. Hardness measurements measure the resistance of a material to deformation under a compressive load. It is often insensitive to a change in coating cohesion. However, the sliding wear behavior of a coating is very sensitive to this aspect. This could explain why the coating hardness results are relatively similar, while the volume losses are different. Almen strips covered with the 7102-2 and 7102-4 coatings were put in a furnace at 400, 600, or

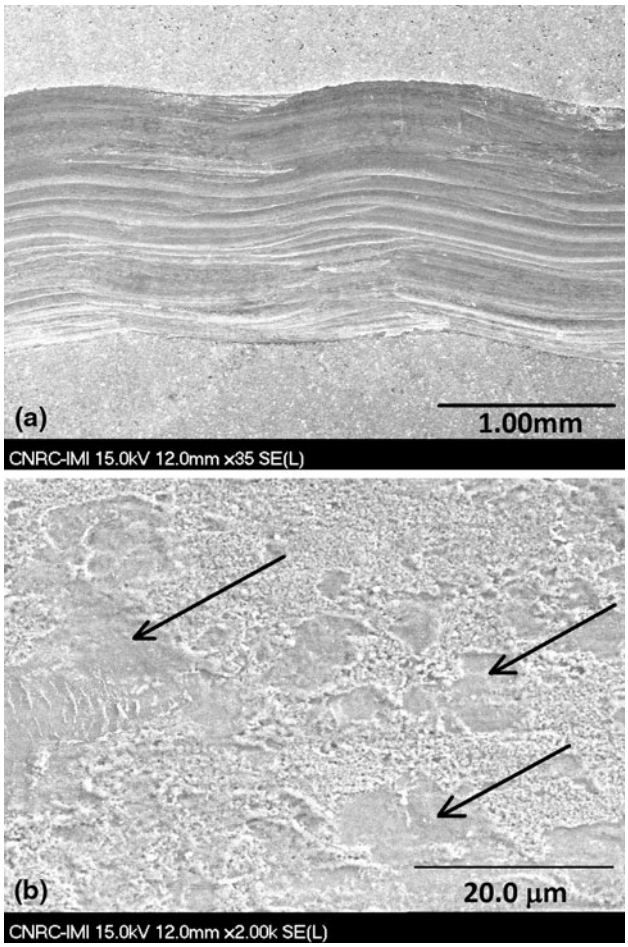

Fig. 9 Wear track of 7102-Set 2 coating: (a) overview and (b) higher magnification

800 °C for 15 minutes and then removed for a natural cool down. In both cases, it was found that while the Almen strips heated at 400 °C keep the same curvature, those heated at 600 and 800 °C are strongly deformed (Fig. 11). The coatings are in tension, potentially indicating a reduction in volume of the coating after heating above 400 °C. This reduction in volume would be another indication of a densification occurring during heating.

Another possibility is that the residual stresses originated during spraying modify the precipitation behavior of the coatings during the ramping up stage toward high temperatures. Compressive or tensile residual stress levels

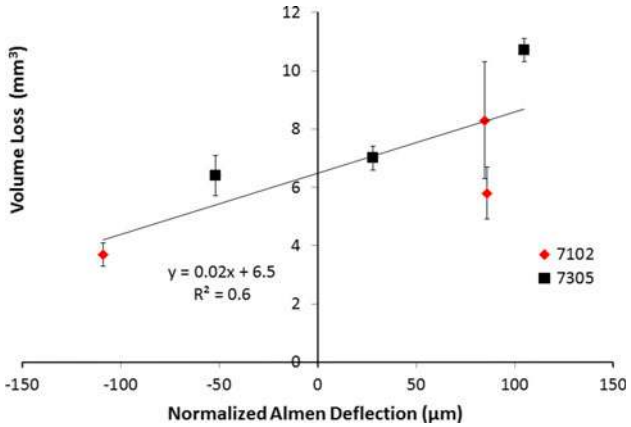

Fig. 10 Volume loss as a function of normalized as-sprayed Almen N deflection

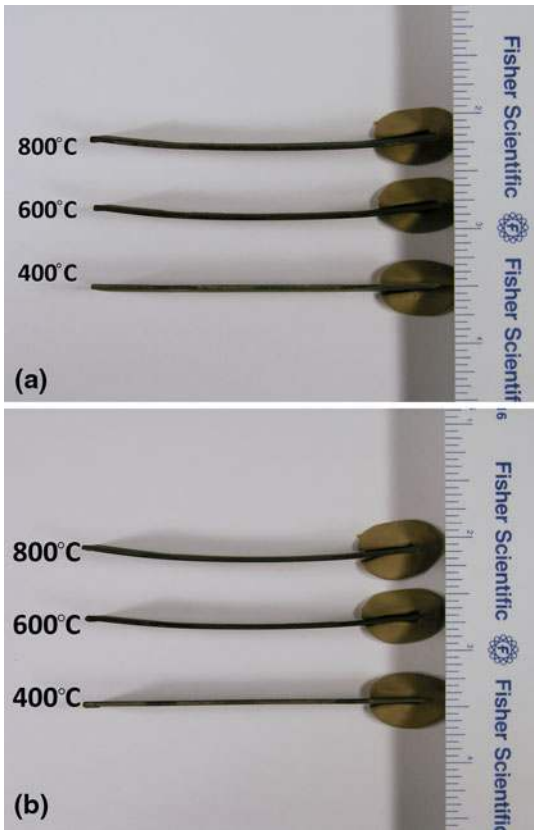

Fig. 11 Almen strips heat treated at 400, 600, and 800 °C: (a) 7102-2 and (b) 7102-4

would change the dimensions of the lattices of the matrix (e.g., Ni-Cr), thereby facilitating or reducing atomic diffusion (Ref 14). Specifically for the 7305 coatings (Tables 4, 5), the Set 3 coating, which exhibits the highest compressive stress level, also exhibits the lowest I_c value (and highest wear resistance) after wear testing at 800 °C. This could be an extra indication that carbide precipitation is affected by the residual stresses. However, further work is needed to validate those hypotheses.

In general, it was found that the powder 7102 produces more wear-resistant coatings than the powder 7305, possibly due to its higher initial carbide content (80% versus 75%). The irregular and porous particles of the 7102 powder do not seem to be detrimental to the coating wear properties.

4. Conclusions

This study was intended to develop a better understanding of the effect of HVOF spraying parameters on the resulting Cr_3Cr_2-20-25wt.%NiCr coating microstructures and wear properties at high temperatures. It was found that spraying parameters that yield higher particle temperatures tend to produce coatings with more pronounced phase degradation, mainly through carbide dissolution. These carbide dissolution levels tend to be more pronounced in denser particles than those of porous ones due to the better thermal conductivity of the denser material. Chromium carbides reprecipitate when the coatings are submitted to high temperatures so that their I_c and microhardness values are increased when compared to those of the as-sprayed coatings. Despite those significant microstructural changes, it appears that the high temperature sliding wear properties of the coatings are not strongly affected by the coating as-sprayed microstructure (initial I_c) and microhardness. In order to maximize the wear resistance of Cr_3C_2-NiCr coatings at high temperatures, spraying parameters can simply be adjusted to favor compressive residual stresses and minimize the level of porosity. For the specific combinations of powders and torch employed in this work, these conditions were achieved by spraying the particles at the average temperature and velocity ranges of ~1700-1800 °C and 750-800 m/s, respectively, at ~20 cm of spray distance.

Acknowledgments

The authors acknowledge the technical assistance of Frédéric Belval, Bernard Harvey, Jean-François Alarie, David de Lagrave, and Michel Thibodeau.

References

1. J.R. Davis, *Handbook of Thermal Spray Technology*, ASM International, Materials Park, OH, 2004
2. M. Roy, A. Pauschitz, J. Wernisch, and F. Franek, The Influence of Temperature on the Wear of Cr3C2-25(Ni20Cr) Coating—Comparison Between Nanocrystalline Grains and Conventional Grains, *Wear*, 2004, **257**(7-8), p 799-811
3. S. Matthews, M. Hyland, and B. James, Long-Term Carbide Development in High-Velocity Oxygen Fuel/High-Velocity Air Fuel Cr3C2-NiCr Coatings Heat Treated at 900°C, *J. Therm. Spray Technol.*, 2004, **13**(4), p 526-536
4. J.M. Guilemany, J.M. Miguel, S. Vizcaıno, C. Lorenzana, J. Delgado, and J. Sánchez, Role of Heat Treatments in the Improvement of the Sliding Wear Properties of Cr3C2-NiCr Coatings, *Surf. Coat. Technol.*, 2002, **157**(2-3), p 207-213

5. V.N. Shukla, V.K. Tewari, and R. Jayaganthan, Comparison of Tribological Behavior of Cr3C2/NiCr Coatings Deposited by Different Thermal Spray Techniques: A Review, *Int. J. Mater. Sci. Eng.*, 2011, **2**(1-2), p 55-58
6. X.M. Li, Y.Y. Yang, T.M. Shao, Y.S. Jin, and G. Barbezat, Impact Wear Performance of Cr3C2-NiCr Coatings by Plasma and HVOF Spraying, *Wear*, 1997, **202**(2), p 208-214
7. G. Barbezat, A.R. Nicoll, and A. Sickinger, Abrasion, Erosion and Scuffing Resistance of Carbide and Oxide Ceramic Thermal Sprayed Coatings for Different Applications, *Wear*, 1993, **162-164**, p 529-537
8. S. Wirojanupatump, P.H. Shipway, and D.G. McCartney, The Influence of HVOF Powder Feedstock Characteristics on the Abrasive Wear Behaviour of CrxCy-NiCr Coatings, *Wear*, 2001, **249**(9), p 829-837
9. S. Matthews, B. James, and M. Hyland, The Role of Microstructure in the Mechanism of High Velocity Erosion of Cr3C2-NiCr Thermal Spray Coatings: Part 1—As-Sprayed Coatings, *Surf. Coat. Technol.*, 2009, **203**(8), p 1086-1093
10. S. Matthews, M. Hyland, and B. James, Microhardness Variation in Relation to Carbide Development in Heat Treated Cr3C2-NiCr Thermal Spray Coatings, *Acta Mater.*, 2003, **51**(14), p 4267-4277
11. S. Matthews, B. James, and M. Hyland, The Role of Microstructure in the Mechanism of High Velocity Erosion of Cr3C2-NiCr Thermal Spray Coatings: Part 2—Heat Treated Coatings, *Surf. Coat. Technol.*, 2009, **203**, p 1094-1100
12. C. Verdon, A. Karimi, and J.L. Martin, A Study of High Velocity Oxy-Fuel Thermally Sprayed Tungsten Carbide Based Coatings, *Mater. Sci. Eng. A*, 1998, **246**(1-2), p 11-24
13. L.M. Berger, M. Woydt, S. Zimmermann, H. Keller, G. Schwier, R. Enžl, and S. Thiele, Tribological Behavior of HVOF-Sprayed Cr3C2-NiCr and TiC-Based Coatings Under High-Temperature Dry Sliding Condition, *Proceedings of the International Thermal Spray Conference*, 2004, p 468-477
14. P. Shewmon, *Diffusion in Solids*, 2nd ed., The Minerals, Metals & Materials Society, Warrendale, PA, 1989